



How to cite this article:

Mohd Ghani, N. A. S., & Jumaat, A. K. (2022). Selective Segmentation Model for Vector-Valued Images. *Journal of Information and Communication Technology*, 21(2), 149-173. <https://doi.org/10.32890/jict2022.21.2.1>

Selective Segmentation Model for Vector-Valued Images

¹Noor Ain Syazwani Mohd Ghani & ^{*2}Abdul Kadir Jumaat

^{1&2}Faculty of Computer and Mathematical Sciences,
Universiti Teknologi MARA, 40450,
Shah Alam, Selangor, Malaysia

²Institute for Big Data Analytics and
Artificial Intelligence (IBDAAI), Kompleks Al-Khawarizmi,
Universiti Teknologi MARA, 40450, Shah Alam, Selangor, Malaysia

2021418828@student.uitm.edu.my

*abdulkadir@tmsk.uitm.edu.my

*Corresponding author

Received: 2/4/2021 Revised: 26/9/2021 Accepted: 20/10/2021 Published: 7/4/2022

ABSTRACT

One of the most important steps in image processing and computer vision for image analysis is segmentation, which can be classified into global and selective segmentations. Global segmentation models can segment whole objects in an image. Unfortunately, these models are unable to segment a specific object that is required for extraction. To overcome this limitation, the selective segmentation model, which is capable of extracting a particular object or region in an image, must be prioritised. Recent selective segmentation models have shown to be effective in segmenting greyscale images. Nevertheless, if the input is vector-valued or identified as a colour image, the models simply

ignore the colour information by converting that image into a greyscale format. Colour plays an important role in the interpretation of object boundaries within an image as it helps to provide a more detailed explanation of the scene's objects. Therefore, in this research, a model for selective segmentation of vector-valued images is proposed by combining concepts from existing models. The finite difference method was used to solve the resulting Euler-Lagrange (EL) partial differential equation of the proposed model. The accuracy of the proposed model's segmentation output was then assessed using visual observation as well as by using two similarity indices, namely the Jaccard (JSC) and Dice (DSC) similarity coefficients. Experimental results demonstrated that the proposed model is capable of successfully segmenting a specific object in vector-valued images. Future research on this area can be further extended in three-dimensional modelling.

Keywords: Active contour, colour image segmentation, selective segmentation, variational model, vector-valued image.

INTRODUCTION

The process of dividing an image into its constituent regions or objects for subsequent processing is known as image segmentation. Image segmentation is necessary to analyse and segment an image into various parts that may be useful for basic applications such as in the fields of robotics, image analysis, medical diagnosis, and object detection (Jumaat & Chen, 2017). The edge-based models and region-based models are two categories of segmentation models. The term "edge-based model" refers to a model that uses an edge detection function to convert original images into edge images. The techniques are useful for shape boundary recognition (Othman et al., 2016). Active Contour Model (ACM) is an effective edge-based algorithm that is widely used in image segmentation to detect objects in an image using curve evolution techniques (Fang et al., 2021). Kass et al. (1988) were the first authors that introduced ACM. They observed the use of the snake model or ACM for interactive interpretation and successfully proved that this model is useful to interactively specify the region of interest within an image. According to Huang and Liu (2015), two major challenges for ACM are: (1) low contrast edges of objects within an image that may lead to inaccurate segmentations; and (2) that ACM is usually sensitive to its initial position. Further improvement was done by Xu and Prince (1998), which later led to

the formulation of the Gradient Vector Flow (GVF) snake model. The model provided substantial improvement in segmentation results and delivered satisfactory results in medical image segmentation (Xu & Prince, 1998).

On the other hand, by separating all pixel values of the object of interest from its corresponding background pixel values (based on image intensity values within a group of neighbouring pixels), the main goal of region-based segmentation techniques is to locate image edges between regions (Mazouzi & Guessoum, 2021). Some classic techniques of region-based segmentation are thresholding (Hore et al., 2016), watershed (Zhang et al., 2017; Xue et al., 2021), region growing (Jiang et al., 2017; Shi et al., 2021), and region splitting and merging (Bala & Sharma, 2017).

The most popular region-based segmentation model is arguably by Mumford and Shah (1989), which is known as the Piecewise Constant (PC) and was established by minimising the variational functional problem of an image. The variational approach can offer high quality processing capabilities for imaging (Dobrosotskaya & Guo, 2017) and often uses the calculus of variations to optimise the function (Yearwood, 2018). However, this model is not a straightforward affair in practice. Therefore, Chan and Vese (1999) developed a reduction and simplification model of the original work from Mumford and Shah (1989). The image $z(x, y)$ according to this modified model is made up of two regions. The unknown contour, Γ , separates the regions. In its simplest form (in the case of two phases segmented into a foreground and a background region), the image will be divided by a piecewise constant function. Chan et al. (2000) then extended their work on greyscale images to vector-valued images. The main difference of this extended method is that it can now segment colour images that it was unable to process in the previous model. Moreover, it offers better output results with extra information that could be extracted. Nevertheless, only the images with homogenous intensity are suitable for this model. Therefore, Vese and Chan (2002) formulated a new Piecewise Smooth (PS) model to overcome the issues related to images with inhomogeneous intensity. Following these variational approaches, many other researchers have proposed new variational models such as Wei et al. (2017), Fang et al. (2018), and Zhao et al. (2018).

In general, all models described above are suitable for the purpose of global segmentation, whereby all objects in the observed image will be segmented. Selective segmentation is concerned with segmenting an object into a specific region with minimal user intervention (Jumaat & Chen, 2017). In 2010, Badshah and Chen combined the global segmentation models by both Chan and Vese (2001) and Mumford and Shah (1989) to form a new selective segmentation oriented model. Additionally, Rada and Chen (2011) introduced the Dual Level Set model to increase the reliability of the initial selective segmentation model. Since the above selective segmentation model uses one set of geometric constraints, Nguyen et al. (2012) proposed an Interactive Image Segmentation (IIS) model that adopted two sets of geometric constraints, namely the geometric points for the inside and outside of the specific object. This model is capable of segmenting an object in both greyscale and vector-valued images. The IIS model (Nguyen et al., 2012) is considered state-of-the-art in segmenting vector-valued images (Ali et al., 2020). Further improvements were made by Rada and Chen (2013) on their existing model. Rada and Chen (2013) and Jumaat and Chen (2019) discovered that a single application of geometric constraint gives better results in segmenting input images as compared to two geometric constraints. The drawback of this model, however, is that it is computationally expensive.

Consequently, Spencer and Chen (2015) proposed a Distance Selective Segmentation (DSS) model. This model performed better and more efficiently as compared to the previous model as it is less sensitive to inputs from the user and has lower computational costs than Rada and Chen's (2013) model. Nevertheless, if the input data is a vector-valued image, the DSS model would ignore the colour information by converting the input image into a greyscale format image. It is important to consider including the colour map data in processing a vector-valued image because it provides richer information such as edge and intensity and therefore could be useful for the domain of pattern recognition and computer vision (Embong et al., 2017).

This research proposes the formulation of a new selective segmentation model for vector-valued or colour images by combining the established models from Spencer and Chen (2015) and Chan et al. (2000). Colour information is embedded in the formulation because it provides additional edge information as compared to greyscale

information. This research focuses on selective image segmentation, as the main objective is to segment only a specific object in an image. The finite difference method will be used to solve the resulting Euler-Lagrange (EL) partial differential equation derived from the proposed model. The performance of the proposed model is then inspected by using visual observation and evaluated using the Dice Similarity Coefficient (DSC) and Jaccard Similarity Coefficient (JSC).

REVIEW OF EXISTING METHODS

In this section, several methods that are significant to this research are reviewed. The first one is the method by Chan and Vese (2001), followed by the methods by Chan et al. (2000) and Spencer and Chen (2015).

The Chan and Vese Model

The variational mathematical model formulation developed by Chan and Vese (2001) is useful in image segmentation. The Chan and Vese (2001) model is abbreviated as the CV model in this research. Let $z = z(x, y)$ be an image. In the CV model, the assumption made is that z is formed by two main regions, whereby the unknown contour Γ separates the regions. Inside the curve or contour Γ , assume the region Ω_1 represents the specific object with the unknown intensity value c_1 . Outside the curve Γ , the image intensity is approximated by the unknown value c_2 in $\Omega_2 = \Omega \setminus \Omega_1$. Then, with $\Omega = \Omega_1 \cup \Omega_2$, the CV model minimises the following Equation 1:

$$\min_{\Gamma, c_1, c_2} \left\{ CV(\Gamma, c_1, c_2) = \mu \text{ length}(\Gamma) + \lambda_1 \int_{\Omega_1} (z - c_1)^2 dx dy + \lambda_2 \int_{\Omega_2} (z - c_2)^2 dx dy \right\} \quad (1)$$

Here, the unknown constants c_1 and c_2 are considered as the approximately piecewise constant intensities of the mean values of z inside and outside the variable contour Γ . The parameters μ , λ_1 and λ_2 , which are non-negative parameters, represent the weights for the regularising term and fitting term, respectively. The level set method was applied by following the idea introduced by Osher et al. (1988). To simplify the notation, they introduced the Heaviside function, $H(\phi(x, y))$ and Dirac delta function, $\delta(\phi(x, y))$ as defined in the following Equations 2 and 3, respectively:

$$H(\phi(x, y)) = \frac{1}{2} \left[1 + \frac{\phi}{\varepsilon} + \frac{1}{\pi} \sin(\pi\phi/\varepsilon) \right]. \quad (2)$$

$$\delta(\phi(x, y)) = \frac{1}{2\varepsilon} \left[1 + \cos\left(\frac{\pi\phi}{\varepsilon}\right) \right]. \quad (3)$$

Here, $\phi(x, y)$ is a level set function, ε is a constant used to avoid the values of $H(\phi(x, y))$, and $\delta(\phi(x, y))$ tends to be zero, which may lead to the failure of the object to be extracted if it is far from the initial contour (Altarawneh et al., 2014).

Therefore, Equation 1 is transformed into the following Equation 4:

$$\min_{\Gamma, c_1, c_2} \left\{ \begin{aligned} CV(\phi, c_1, c_2) = \mu \int_{\Omega} |\nabla H(\phi)| dx dy + \lambda_1 \int_{\Omega} (z - c_1)^2 H(\phi) dx dy \\ + \lambda_2 \int_{\Omega} (z - c_2)^2 (1 - H(\phi)) dx dy. \end{aligned} \right\} \quad (4)$$

Let the function ϕ be fixed. Then, Equation 4 is minimised with respect to c_1 and c_2 that yields the following Equation 5:

$$\left. \begin{aligned} c_1 &= \int_{\Omega} z(x, y) H(\phi(x, y)) d\Omega / \int_{\Omega} H(\phi(x, y)) d\Omega \\ c_2 &= \int_{\Omega} z(x, y) (1 - H(\phi(x, y))) d\Omega / \int_{\Omega} (1 - H(\phi(x, y))) d\Omega. \end{aligned} \right\} \quad (5)$$

Fixing c_1 and c_2 as constants in $CV(\phi, c_1, c_2)$ leads to the following Equation 6:

$$\left\{ \begin{aligned} \mu \delta(\phi) \nabla \cdot \left(\frac{\nabla \phi}{|\nabla \phi|} \right) - \lambda_1 \delta(\phi) (z - c_1)^2 + \lambda_2 \delta(\phi) (z - c_2)^2 &= 0 \text{ in } \Omega, \\ \frac{\delta(\phi)}{|\nabla \phi|} \frac{\partial u}{\partial \bar{n}} &= 0 \text{ on } \partial\Omega, \end{aligned} \right. \quad (6)$$

where $\nabla \phi$ represents the gradient of the level set function ϕ . Equation 6 is called the EL equation, which was solved using the finite difference method. However, the CV model is limited to only greyscale images.

The Chan-Sandberg-Vese Model

Chan et al. (2000) formulated a variational-based ACM for colour or vector-valued images known as the Chan-Sandberg-Vese (CSV) model. The model is an extension of the CV model for the case of vector-valued images. The CSV model minimised Equation 1 of the CV model over the length (the first term) of the contour, plus the sum of the fitting error (the second and the third terms) for each component of a vector-valued image. By letting $u_{0,i}$ as the i -th channel of a vector-

valued image on the domain Ω , with $i=1, \dots, N$ channels and letting C as the evolving curve and defining the two unknown constant vectors as $\bar{c}^+ = (c_1^+, \dots, c_N^+)$ and $\bar{c}^- = (c_1^-, \dots, c_N^-)$, the CSV formulation is defined as the following Equation 7:

$$CSV(\phi, \bar{c}^+, \bar{c}^-) = \mu \int_{\Omega} \delta(\phi(x, y)) |\nabla \phi(x, y)| d\Omega \quad (7)$$

$$+ \int_{in(C)} \frac{1}{N} \sum_{i=1}^N \lambda_i^+ |u_{0,i}(x, y) - c_i^+|^2 d\Omega + \int_{out(C)} \frac{1}{N} \sum_{i=1}^N \lambda_i^- |u_{0,i}(x, y) - c_i^-|^2 d\Omega.$$

Here, the parameters λ_i^+ and λ_i^- are non-negative parameters that represent the weight for the fitting term, while the parameter μ is a non-negative parameter that represents the weight for length term. For vector-valued images, the constants \bar{c}^+ and \bar{c}^- are the mean of the colour values inside and outside the segmented image. Equation 7 can be written in level set representation as in the following Equation 8:

$$CSV(\phi, \bar{c}^+, \bar{c}^-) = \mu \int_{\Omega} \delta(\phi) |\nabla \phi| dx dy + \int_{\Omega} \frac{1}{N} \sum_{i=1}^N \lambda_i^+ |u_{0,i} - c_i^+|^2 H(\phi) dx dy \quad (8)$$

$$+ \int_{\Omega} \frac{1}{N} \sum_{i=1}^N \lambda_i^- |u_{0,i} - c_i^-|^2 (1 - H(\phi)) dx dy,$$

for $i = 1, \dots, N$. The sensitivity of the object detector can be tuned by the parameters μ and $\bar{\lambda}^{+,-} = (\lambda_1^{+,-}, \dots, \lambda_N^{+,-})$. It was suggested that the large μ or small $\bar{\lambda}$ can be considered to filter the high noise frequency in the model. Otherwise, to segment objects with fine details, a larger value of $\bar{\lambda}$ can be considered. The functions H and δ are similarly defined as Equations 2 and 3, respectively. By minimising the functions with respect to c_i^+ and c_i^- , for $i = 1, \dots, N$, the following Equation 9 is obtained:

$$\left. \begin{aligned} c_i^+ &= \int_{\Omega} u_{0,i}(x, y) H(\phi(x, y)) dx dy / \int_{\Omega} H(\phi(x, y)) dx dy \\ c_i^- &= \int_{\Omega} u_{0,i}(x, y) (1 - H(\phi(x, y))) dx dy / \int_{\Omega} (1 - H(\phi(x, y))) dx dy \end{aligned} \right\} \quad (9)$$

After that, by assuming \bar{c}^+ and \bar{c}^- as constants in $CSV(\phi, \bar{c}^+, \bar{c}^-)$, the EL equation is obtained and defined as the following Equation 10:

$$\frac{\partial \phi}{\partial t} = \delta(\phi) \left[\mu \cdot \text{div} \left(\frac{\nabla \phi}{|\nabla \phi|} \right) - \frac{1}{N} \sum_{i=1}^N \lambda_i^+ (u_{0,i} - c_i^+)^2 + \frac{1}{N} \sum_{i=1}^N \lambda_i^- (u_{0,i} - c_i^-)^2 \right]. \quad (10)$$

The term $|\nabla \phi|$ represents the norm of the gradient of the level set function ϕ that ensures the smoothness of the generated curve. Then, the model was solved using the finite difference method.

Spencer-Chen Model

A new formulation for the selective model was developed by Spencer and Chen (2015), termed the DSS model. Let $z(x, y)$ be a greyscale image. The marker set is given as $A = \{w_i = (x_i^*, y_i^*) \in \Omega, 1 \leq i \leq n_1\}$ with $n_1 (\geq 3)$ marker points. The polygon P is constructed by using set A that links up the markers. In the model, the normalised Euclidean distance, $P_d(x, y)$ of each point $(x, y) \in \Omega$ from its nearest point in the polygon, made up of $(x_p, y_p) \in P$, constructed from user input set, A , was introduced. The function $P_d(x, y)$ is defined as the following Equation 11:

$$P_d(x, y) = \frac{P_0(x, y)}{\|P_0\|_{L^\infty}} \quad (11)$$

where $P_0(x, y) = \sqrt{(x - x_p)^2 + (y - y_p)^2}$. Then, the DSS formulation is given as the following Equation 12:

$$DSS(\Gamma, c_1, c_2) = \mu |\Gamma| + \theta \int_{in(\Gamma)} P_d(x, y) d\Omega + \lambda \int_{in(\Gamma)} (z - c_1)^2 d\Omega + \lambda \int_{out(\Gamma)} (z - c_2)^2 d\Omega. \quad (12)$$

In the level set representation, Equation 12 can be written as the following Equation 13:

$$\min_{\phi, c_1, c_2} \left\{ DSS(\phi, c_1, c_2) = \mu \int_{\Omega} \delta(\phi) |\nabla \phi| d\Omega + \theta \int_{\Omega} H(\phi) P_d d\Omega + \lambda \int_{\Omega} H(\phi) (z - c_1)^2 d\Omega + \lambda \int_{\Omega} (1 - H(\phi)) (z - c_2)^2 d\Omega \right\}, \quad (13)$$

for non-negative parameters θ and μ . Here, θ is the area parameter that controls the weight of the fitting term, while the parameter μ controls the length of the generated curve. It was suggested that the chosen value θ is different for each image and the value is dependent on the targeted object. Normally, a small value θ is needed for a simple image while a large value θ is suitable for a low contrast image close to the neighbouring area.

THE PROPOSED MODEL

The DSS model is not designed to segment colour images. Therefore, the main idea of this research is to propose a new selective segmentation model for vector-valued images, termed Distance

Selective Segmentation 2 (DSS2). The current research combined ideas from the existing models, which were the CSV and DSS models, to formulate the proposed DSS2 model. Here, on images z , geometrical points $n_1 (\geq 3)$ were assumed by the marker set $B = \{w_j = (x_j^*, y_j^*) \in \Omega, 1 \leq j \leq n_1\}$. The polygon P was constructed by using set B . Let the function $P_d(x, y)$ be the Euclidean distance that is the distance of each point $(x, y) \in \Omega$ from its nearest points of $(x_p, y_p) \in P$, constructed from the user input set B defined as the following Equation 14:

$$P_d(x, y) = \sqrt{(x - x_p)^2 + (y - y_p)^2}. \quad (14)$$

Then, the proposed DSS2 model is defined as the following Equation 15:

$$\begin{aligned} DSS2(\Gamma, c_1^i, c_2^i) = & \mu \text{Length}(\Gamma) + \int_{in(\Gamma)} \frac{1}{N} \sum_{i=1}^N \lambda_1^i (z^i(x, y) - c_1^i)^2 d\Omega \\ & + \int_{out(\Gamma)} \frac{1}{N} \sum_{i=1}^N \lambda_2^i (z^i(x, y) - c_2^i)^2 d\Omega + \int_{in(\Gamma)} \theta P_d(x, y) d\Omega, \end{aligned} \quad (15)$$

Where c_1^i and c_2^i are unknown constants that represent the average value of z^i inside and outside the unknown curve, respectively. The non-negative parameters of μ , λ_1^i , and λ_2^i are weights for the regularising term and fitting term, respectively. Then, by introducing the level set function $\phi(x, y)$, Equation 15 can be written as the following Equation 16:

$$\begin{aligned} & \min_{\phi, c_1^i, c_2^i} DSS2^{LS}(\phi, c_1^i, c_2^i), \\ DSS2^{LS}(\phi, c_1^i, c_2^i) = & \mu \int_{\Omega} \delta(\phi) |\nabla \phi| d\Omega + \int_{\Omega} \frac{1}{N} \sum_{i=1}^N \lambda_2^i (1 - H(\phi)) (z^i - c_2^i)^2 d\Omega \\ & + \int_{\Omega} \frac{1}{N} \sum_{i=1}^N \lambda_1^i H(\phi) (z^i - c_1^i)^2 d\Omega + \int_{\Omega} \theta H(\phi) P_d d\Omega, \end{aligned} \quad (16)$$

where $\phi(x, y)$, $P_d(x, y)$ and $z^i(x, y)$ are replaced with ϕ , P_d , and z^i , respectively for simplicity and $|\nabla \phi| = \sqrt{\phi_x^2 + \phi_y^2}$. The function ϕ is fixed and Equation 16 is minimised to obtain c_1^i and c_2^i as defined in the following Equations 17 and 18, respectively:

$$c_1^i(\phi) = \frac{\int_{\Omega} z^i H(\phi) dx dy}{\int_{\Omega} H(\phi) dx dy} \quad (\text{average}(z^i) \text{ on } \phi \geq 0). \quad (17)$$

$$c_2^i(\phi) = \frac{\int_{\Omega} z^i (1 - H(\phi)) dx dy}{\int_{\Omega} H(\phi) dx dy} \quad (\text{average}(z^i) \text{ on } \phi < 0). \quad (18)$$

In order to derive the EL equation for ϕ , both H and δ are defined as the following Equations 19 and 20, respectively:

$$H(\phi(x, y)) = \begin{cases} 1 & \text{if } \phi > \varepsilon \\ 0 & \text{if } \phi < -\varepsilon \\ \frac{1}{2} \left[1 + \frac{\phi}{\varepsilon} + \frac{1}{\pi} \sin(\pi\phi/\varepsilon) \right] & \text{if } |\phi| \leq \varepsilon, \end{cases} \quad (19)$$

$$\delta(\phi) = H'_\varepsilon(\phi) = \frac{1}{2\varepsilon} \left[1 + \cos\left(\frac{\pi\phi}{\varepsilon}\right) \right] \text{ if } |\phi| \leq \varepsilon. \quad (20)$$

Then, by fixing constant c_1^i and c_2^i , the EL equation with respect to ϕ is given by the following Equation 21:

$$\begin{cases} \frac{\partial \phi}{\partial t} = \delta(\phi) \left[\mu \operatorname{div} \left(\frac{\nabla \phi}{|\nabla \phi|} \right) - \frac{1}{N} \sum_{i=1}^N \lambda_1^i (z^i - c_1^i)^2 + \frac{1}{N} \sum_{i=1}^N \lambda_2^i (z^i - c_2^i)^2 - \theta P_d \right] & \text{in } \Omega, \\ \frac{\delta(\phi)}{|\nabla \phi|} \frac{\partial \phi}{\partial \vec{n}} = 0 & \text{on } \partial\Omega, \end{cases} \quad (21)$$

where \vec{n} is the exterior normal at the boundary of $\partial\Omega$ and $\partial\phi/\partial\vec{n}$ is the normal derivative of ϕ at the boundary. The finite difference scheme was used to solve this EL equation problem.

NUMERICAL IMPLEMENTATION

This section describes the semi-implicit finite difference scheme to solve the EL equation given in Equation 21. The evolution of ϕ is discretised according to the following Equation 22:

$$\frac{\partial \phi_{i,j}}{\partial t} = \delta(\phi_{i,j}) \left[\mu(K_{i,j}) - \frac{1}{N} \sum_{i=1}^N \lambda_1^i (z_{i,j}^i - c_1^i)^2 + \frac{1}{N} \sum_{i=1}^N \lambda_2^i (z_{i,j}^i - c_2^i)^2 - \theta P_d \right], \quad (22)$$

where δ is computed according to Equation 20 and the curvature, $K_{i,j}$ is defined as the following Equation 23:

$$K_{i,j} = \operatorname{div} \left(\frac{\nabla \phi}{|\nabla \phi|} \right) = \frac{\phi_{ii} \phi_j^2 - 2\phi_{ij} \phi_i \phi_j + \phi_{jj} \phi_i^2}{(\phi_i + \phi_j)^{3/2}}, \quad (23)$$

where ϕ_i , ϕ_j and ϕ_{ij} are derivatives of the level set ϕ . Here, the forward finite difference method is used to obtain $\phi_i = \frac{\phi_{i+\Delta i, j} - \phi_{i, j}}{\Delta i}$, $\phi_j = \frac{\phi_{i, j+\Delta j} - \phi_{i, j}}{\Delta j}$,

$$\phi_{ii} = \frac{\phi_{i+\Delta i, j} - 2\phi_{i, j} + \phi_{i-\Delta i, j}}{\Delta i \Delta i}, \quad \phi_{jj} = \frac{\phi_{i, j+\Delta j} - 2\phi_{i, j} + \phi_{i, j-\Delta j}}{\Delta j \Delta j}, \quad \text{and } \phi_{ij} = \frac{(\phi_{i+\Delta i, j+\Delta j} - \phi_{i, j+\Delta j}) - (\phi_{i+\Delta i, j} - \phi_{i, j})}{\Delta i \Delta j}.$$

Let $\Delta i = \Delta j = 1$ be the space steps, then $\phi_i = \phi_{i+1,j} - \phi_{i,j}$, $\phi_{ii} = \phi_{i+1,j} - 2\phi_{i,j} + \phi_{i-1,j}$, $\phi_{jj} = \phi_{i,j+1} - 2\phi_{i,j} + \phi_{i,j-1}$, and $\phi_{ij} = \phi_{i+1,j+1} - \phi_{i,j+1} - \phi_{i+1,j} + \phi_{i,j}$. Subsequently, Equation 22 can be further written as the following Equation 24:

$$\begin{aligned} \frac{\partial \phi_{i,j}}{\partial t} = \delta(\phi_{i,j}) \left[\mu(K_{i,j}) - \frac{1}{N} \sum_{i=1}^N \lambda_1^i (z_{i,j}^i - c_1^i)^2 \right. \\ \left. + \frac{1}{N} \sum_{i=1}^N \lambda_2^i (z_{i,j}^i - c_2^i)^2 - \theta P_d \right], \quad i, j = 1, \dots, M-1, \end{aligned} \quad (24)$$

There are other ways to discretise Equation 21; however, the above form is simpler according to Yue (2009). Moreover, Getreuer (2012) stated that central differences are undesirable in a discretised optimisation approach since they miss the thin image structure. Next, the semi-implicit Gauss-Seidel method was applied in Equation 24 to produce the following Equation 25:

$$\begin{aligned} \frac{\phi_{i,j}^{n+1} - \phi_{i,j}^n}{dt} = \delta(\phi_{i,j}^n) \left[\mu(K_{i,j}^n) - \frac{1}{N} \sum_{i=1}^N \lambda_1^i (z_{i,j}^i - c_1^i(\phi_{i,j}^n))^2 \right. \\ \left. + \frac{1}{N} \sum_{i=1}^N \lambda_2^i (z_{i,j}^i - c_2^i(\phi_{i,j}^n))^2 - \theta P_d \right] \end{aligned} \quad (25)$$

The Neumann boundary condition can be implemented in the following way:

$$\begin{aligned} \phi_{0,j}^n = \phi_{1,j}^n, \quad \phi_{M,j}^n = \phi_{M-1,j}^n, \quad \phi_{i,0}^n = \phi_{i,1}^n, \quad \phi_{i,M}^n = \phi_{i,M-1}^n, \quad \phi_{0,0}^n = \phi_{1,1}^n, \quad \phi_{0,M}^n = \phi_{1,M-1}^n, \\ \phi_{M,0}^n = \phi_{M-1,1}^n, \quad \phi_{M,M}^n = \phi_{M-1,M-1}^n. \end{aligned}$$

Steps of Algorithm for the Proposed Model

Algorithm 1 shows the steps involved to implement the new proposed model, DSS2, to compute the solution using the MATLAB software.

Algorithm 1: DSS2 Algorithm

1. Set values of parameters μ, θ, λ and define the marker set B. Then, calculate $P_d(x, y)$ using Equation 14.
 2. Initialise ϕ^0 , $n = 0$.
 3. Compute $c_1^i(\phi^n)$ and $c_2^i(\phi^n)$ as the region averages given in Equations 17 and 18, respectively.
 4. Solve for ϕ from the EL equation in Equation 25 to obtain ϕ^{n+1} .
 5. If $\|\phi^{n+1} - \phi^n\| / \|\phi^n\| \leq tol$ or maximum iteration (*maxit*) reaches 3,000 iterations, then stop. Otherwise, repeat Steps 3 and 4. Here, the value of tolerance is set as $tol = 0.005$, which is sufficient for curve evolution to all models used in the experiments.
-

EXPERIMENTS AND RESULTS

Two experiments were carried out. In Experiment 1, the segmentation accuracy of the existing CSV and IIS models was compared with the proposed model, which was the DSS2 model, in segmenting a targeted object in each synthetic test image. While in Experiment 2, real test images were used. The segmentation performance of all the models was evaluated using two approaches. The first approach was the qualitative approach, whereby the segmentation performance of all models was evaluated by visual observation. The second approach was the quantitative approach, whereby two similarity coefficients, namely Jaccard (JSC) and Dice (DSC) were computed such that. $JSC = |S_n \cap S_*| / |S_n \cup S_*|$ and $DSC = 2|S_n \cap S_*| / (|S_n| + |S_*|)$. Here, the set of the segmented domain Ω_1 was denoted by S_n while the true set of Ω_1 was denoted by S_* . The return values of JSC and DSC were in the range of $[0,1]$. A perfect segmentation quality was indicated by a value of 1 while poor quality of segmentation was indicated by a value of 0.

In the following experiments, the values of parameters are as such for all experiments: $\mu = \lambda_1^i = \lambda_2^i = 1$, $tol = 0.005$, and $maxit = 3000$. Here, the time step was set at $dt = 10^{-3}$ since it gave a satisfactory result for segmentation. Besides, $\varepsilon = 10^{-5}$ was taken to avoid singularity or the undefined value problem, which might lead to the failure of the object to be extracted if it were far from the initial contour.

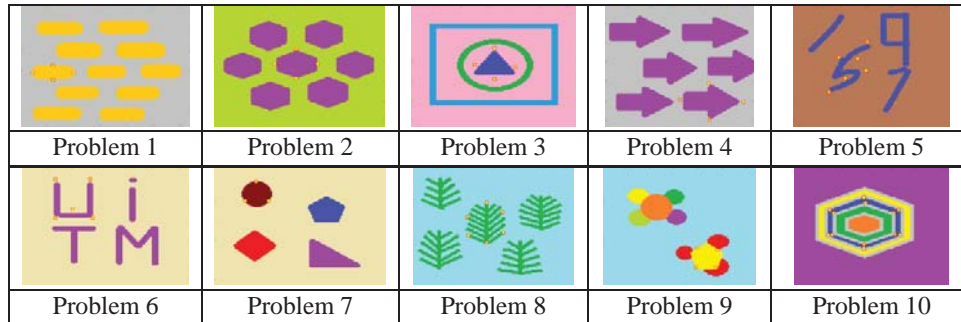
To obtain a satisfactory result, a suitable value of the parameter θ and the user-defined marker points were adjusted. The selection was based on the image and was used to restrict only the specific object. For the case where an object is near to a neighbouring area, the value of θ should be larger, while a small value of θ is needed to segment a clearly separated object.

Experiment 1: Segmentation on Synthetic Images

There were ten synthetic images in this first experiment. The test images are listed in Figure 1. The yellow markers indicate the targeted object.

Figure 1

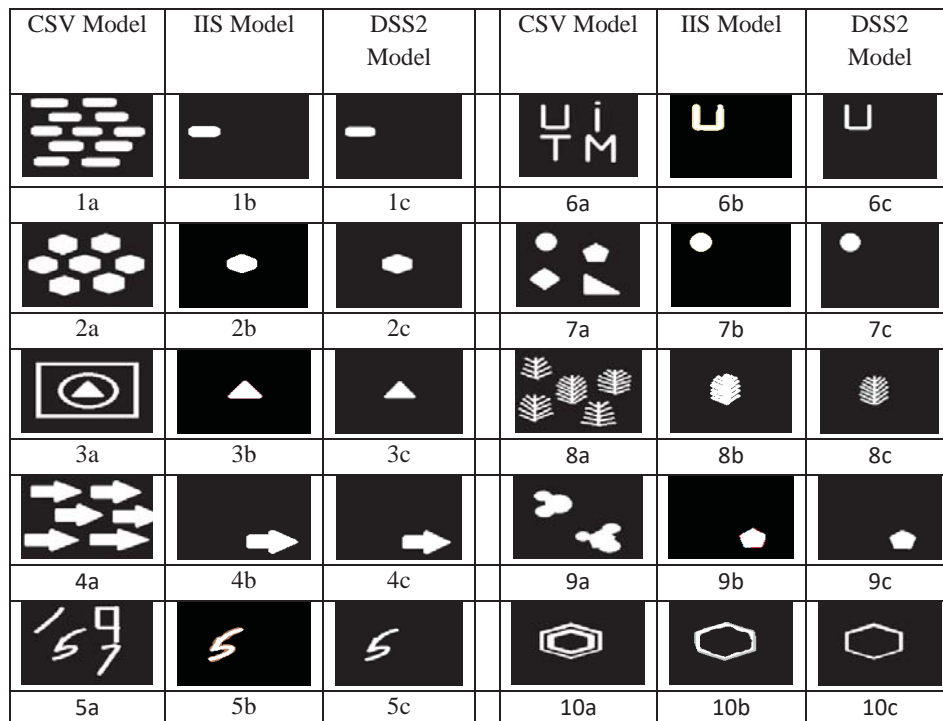
Synthetic Images with Markers



All the test images in Figure 1 were created using the Microsoft Paint software. The accuracy of segmentation for the CSV and IIS models was compared with the proposed model, DSS2, on all ten problems by visual inspection and computation of the JSC and DSC values. Figure 2 demonstrates the segmentation results of each model for all problems in binary form.

Figure 2

Segmentation Results of Experiment 1 for CSV, IIS, and the Proposed DSS2 Models



In Experiment 1, the values of the parameter θ for the DSS2 model were in the range of $\theta = [400, 3600]$. By visual observation, the IIS and DSS2 models were capable of segmenting only the targeted object.

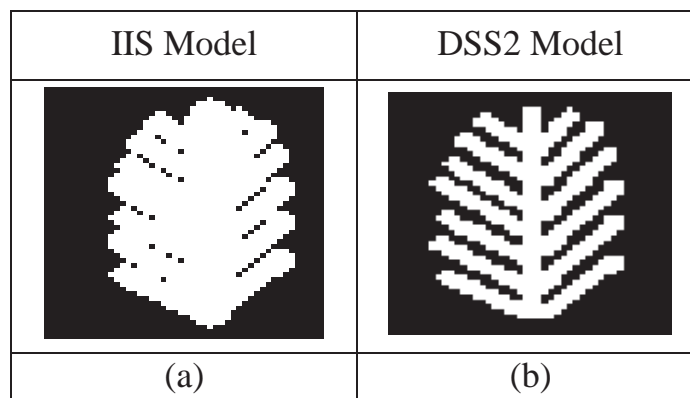
Meanwhile, for images with more than one object, the CSV model failed to segment only the targeted object since multiple objects in the image were segmented, which is known as an over-segmented problem. This mainly occurs because there is no constraint function defined in the formulation of the CSV model to capture a particular object, thus the CSV model will try to segment all objects in each image. However, this is not guaranteed due to the non-convex formulation as can be observed in Figure 2(9a), where the CSV model was unable to segment all objects in Problem 9.

The existing IIS model (Nguyen et al., 2012) is known as a state-of-the-art model capable of generating accurate segmentation results. In general, the IIS model successfully segmented all images and the results were almost similar to the DSS2 model.

However, it was observed that the IIS model was unable to segment Problem 8 in a clean way. Figure 3 demonstrates the zoomed segmentation results of Figures 2(8b) and 2(8c), which represent the segmentation results of Problem 8 for the IIS and DSS2 models, respectively.

Figure 3

Zoomed Segmentation of Problem 8 for IIS and DSS2 Models



The zoomed segmentation results in Figure 3(a) demonstrated the limitation of the IIS model, while the DSS2 model gave a cleaner

segmentation result as illustrated in Figure 3(b). According to Nguyen et al. (2012), the IIS model was unable to segment semi-transparent boundaries and sophisticated shapes (such as bush branches or hair) in a clean way due to its underlying assumption in the hard segmentation formulation that the shape of the targeted object was smooth and could be described by the weighted shortest boundary length.

On the other hand, DSS2 gave a better result because of the existence of the Euclidean distance from the generated polygon region in the formulation. This is helpful to provide a good approximation as the function allowed the solution to be constrained by surrounding values associated with the polygon region, which was constructed by the markers around the targeted object.

Besides qualitative analysis by visual observation, a quantitative analysis of the segmentation accuracy was also provided by evaluating the JSC and DSC values. Table 1 shows the JSC and DSC values of each model for all problems in Experiment 1.

Table 1

The JSC and DSC Values of Experiment 1 for Each Model.

Test Image	CSV Model		IIS Model		DSS2 Model	
	JSC	DSC	JSC	DSC	JSC	DSC
Problem 1	0.09	0.16	1.00	1.00	1.00	1.00
Problem 2	0.14	0.25	0.97	0.98	1.00	1.00
Problem 3	0.16	0.27	1.00	1.00	1.00	1.00
Problem 4	0.17	0.29	1.00	1.00	1.00	1.00
Problem 5	0.30	0.50	0.98	0.99	1.00	1.00
Problem 6	0.28	0.44	1.00	1.00	1.00	1.00
Problem 7	0.21	0.34	1.00	1.00	1.00	1.00
Problem 8	0.25	0.40	0.65	0.79	1.00	1.00
Problem 9	0.26	0.42	0.99	1.00	0.99	0.99
Problem 10	0.50	0.66	0.87	0.93	1.00	1.00
Average	0.236	0.373	0.946	0.969	0.999	0.999

From Table 1, the average JSC and DSC values for DSS2 were 0.999, which was higher than the CSV and IIS models. It was remarked that

the IIS model also delivered a promising result, except for Problem 8 that had a sophisticated shape as explained above. Therefore, the findings indicated that the DSS2 model had the highest average segmentation accuracy in Experiment 1 as compared to the CSV and IIS models.

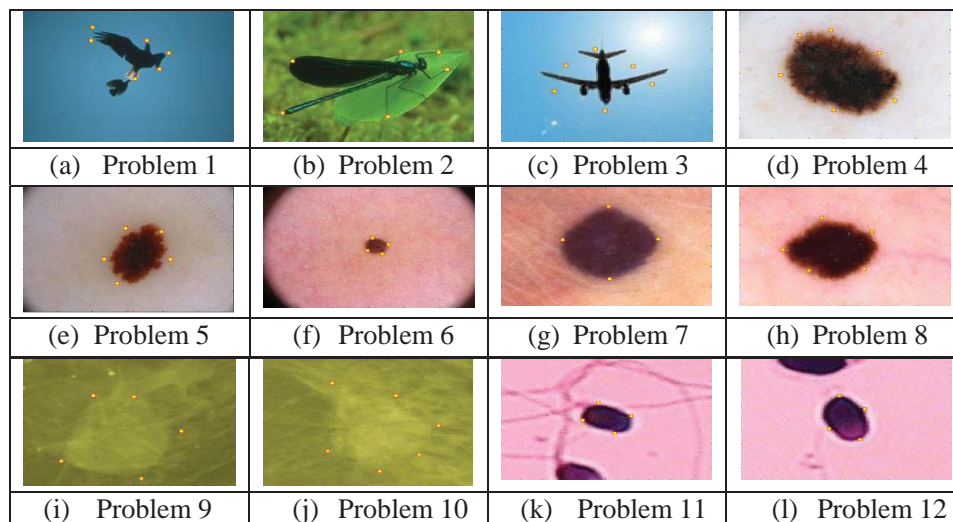
All test images in Experiment 1 were synthetic images. In Experiment 2, the segmentation accuracy of the existing CSV and IIS models was compared with the proposed DSS2 model in segmenting a targeted object in real images.

Experiment 2: Segmentation on Real Images

There were 12 real images in this second experiment. Figure 4 demonstrates the real images with markers in yellow to indicate the targeted object. Problems 1–3 in Figure 4 were obtained from Berkeley’s segmentation dataset and benchmark (Li et al., 2013; Martin et al., 2001); Problems 4–8 were obtained from a publicly accessible dermatology image analysis benchmark (Codella et al., 2018); Problems 9 and 10 were obtained from a mammography image database (Moreira et al., 2012) in yellow colour map to enhance the mass-like patterns; while Problems 11 and 12 were obtained from the Human Sperm Head Morphology dataset (Shaker et al., 2017).

Figure 4

Real Images with Markers







































It was remarked that these real images were very challenging for the segmentation task. This is because the images had intensity inhomogeneity and irregularity boundaries. In addition, Problems 1, 2, 9, and 10 in Figures 4(a), 4(b), 4(i), and 4(j), respectively, had complex shapes.

The accuracy of segmentation for all models on the 12 problems was compared by visual inspection. For quantitative analysis, only the JSC and DSC values of all models were computed in segmenting Problems 1–10 because the ground truth solutions for Problems 11 and 12 were not available. Figure 5 shows the segmentation results of each model for all problems in binary representation.

Figure 5

Segmentation Results of Experiment 2 for CSV, IIS, and the Proposed DSS2 Models

CSV Model	IIS Model	DSS2 Model	CSV Model	IIS Model	DSS2 Model
					
1a	1b	1c	7a	7b	7c
					
2a	2b	2c	8a	8b	8c
					
3a	3b	3c	9a	9b	9c
					
4a	4b	4c	10a	10b	10c
					
5a	5b	5c	11a	11b	11c
					
6a	6b	6c	12a	12b	12c

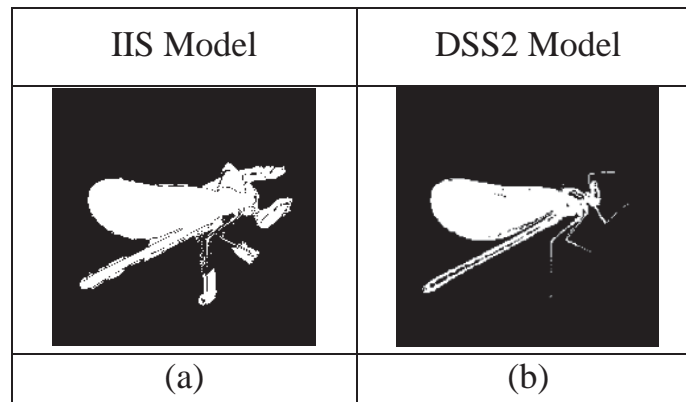
In Experiment 2, the values of the parameter θ for the DSS2 model were in the range of $\theta = [50, 3600]$. By visual inspection, a similar scenario as in Experiment 1 could be observed, whereby the IIS and DSS2

models were capable of segmenting only the targeted object while the CSV model segmented every object in the image.

It was observed that the IIS model was unable to segment the legs of the creature in Problem 2 properly. The following Figure 6 illustrates the zoomed segmentation results of Figures 5(2b) and 5(2c), which represent the segmentation results of Problem 2 for the IIS and DSS2 models, respectively.

Figure 6

Zoomed Segmentation of Problem 2 for IIS and DSS2 Models



The legs of the creature in Problem 2 of Figure 4(b) had a hair-like shape with semi-transparent boundaries. The IIS model was unable to give a clean segmentation as demonstrated in Figure 6(a) as compared to the DSS2 model in Figure 6(b). The accuracy of the segmentation’s performance for all models was also evaluated using JSC and DSC for quantitative analysis. Here, only the values for Problems 1–10 were provided, as the ground truth solutions for Problems 11 and 12 were not available. The values are summarised in Table 2.

Table 2

The JSC and DSC Values of Experiment 2 for Each Model

Test Image	CSV Model		IIS Model		DSS2 Model	
	JSC	DSC	JSC	DSC	JSC	DSC
Problem 1	0.70	0.82	0.83	0.91	0.84	0.91
Problem 2	0.63	0.78	0.68	0.81	0.81	0.89

(continued)

Test Image	CSV Model		IIS Model		DSS2 Model	
	JSC	DSC	JSC	DSC	JSC	DSC
Problem 3	0.91	0.95	0.71	0.83	0.91	0.95
Problem 4	0.91	0.95	0.85	0.92	0.91	0.95
Problem 5	0.83	0.91	0.84	0.91	0.85	0.92
Problem 6	0.11	0.20	0.88	0.94	0.87	0.93
Problem 7	0.97	0.99	0.94	0.97	0.98	0.99
Problem 8	0.87	0.93	0.82	0.90	0.87	0.93
Problem 9	0.60	0.75	0.79	0.88	0.86	0.92
Problem 10	0.48	0.65	0.79	0.88	0.84	0.91
Average	0.701	0.793	0.813	0.895	0.874	0.930

Table 2 demonstrates that the average values of JSC and DSC for the proposed DSS2 model were higher than the CSV and IIS models. Nevertheless, for Problem 6, the IIS model was slightly better than the DSS2 model with an insignificant difference. Overall, the DSS2 model had the highest average segmentation accuracy in Experiment 2 as compared to the CSV and IIS models.

CONCLUSION

In this research, the target was to extract the specific object in an image by using the selective segmentation technique in the vector-valued environment since it carried richer image information in addition to intensity. Therefore, the new mathematical model on selective segmentation of vector-valued images, DSS2, was formulated by combining the ideas from Spencer and Chen (2015) and Chan et al. (2000). The resulting EL equation was derived from the new proposed model and was solved using the finite difference method. Next, the algorithm was implemented by developing the MATLAB coding using the MATLAB R2018 software.

Two experiments were carried out whereby a total of 22 test images were presented to demonstrate the comparison of the proposed DSS2 model with existing models, which were the CSV and IIS models. In Experiment 1, ten synthetic images were tested, while in Experiment 2, 12 real images were tested. Through the qualitative approach (visual inspection), it was found that for all tested images with multiple objects, the CSV model failed to selectively segment the targeted

object and the segmentation output was over-segmented, while DSS2 successfully segmented the targeted object. Other than that, the IIS model was able to selectively segment the targeted object. However, for images with semi-transparent boundaries and sophisticated shapes (such as bush branches or hair), the method was unable to deliver a clean output as compared to the DSS2 model.

For quantitative analysis, the JSC and DSC values were computed for all models to measure the segmentation accuracy. On average, the segmentation performance of the DSS2 model was higher than the CSV and IIS models as indicated by the average values of JSC and DSC for both experiments. Therefore, this led to the conclusion that the DSS2 model provided more satisfactory results in segmenting the object in an image as compared to the CSV and IIS models.

The proposed DSS2 model gave better results because of the existence of the Euclidean distance function, generated by a polygon region in the formulation. Consequently, this function is helpful in providing a good segmentation estimation as the function allows the solution to be constrained by the polygon region, constructed by the markers around the targeted object.

For future works, the research will be extended in three-dimensional formulation and will propose an efficient algorithm in solving the two-dimensional and three-dimensional segmentation problems based on the research by Jumaat and Chen (2020).

ACKNOWLEDGMENT

This work was supported by the Geran Penyelidikan Khas (GPK) Universiti Teknologi MARA Shah Alam, grant number 600-RMC/GPK 5/3 (185/2020), 2020.

REFERENCES

Ali, H., Faisal, S., Chen, K., & Rada, L. (2020). Image-selective segmentation model for multi-regions within the object of interest with application to medical disease. *Visual Computer*, 37(5), 939–955. <https://doi.org/10.1007/s00371-020-01845-1>

- Altarawneh, N. M., Luo, S., Regan, B., Sun, C., & Jia, F. (2014). Global threshold and region-based active contour model for accurate image segmentation. *Signal & Image Processing*, 5(3), 1–11. <https://doi.org/http://dx.doi.org/10.5121/sipij.2014.5301>
- Badshah, N., & Chen, K. (2010). Image selective segmentation under geometrical constraints using an active contour approach. *Communications in Computational Physics*, 7(4), 759–778. <https://doi.org/http://dx.doi.org/10.4208/cicp.2009.09.026>
- Bala, A., & Sharma, A. K. (2017). Split and merge: A region based image segmentation. *International Journal of Emerging Research in Management and Technology*, 6(8), 306–309. <https://doi.org/http://dx.doi.org/10.23956/ijermt.v6i8.157>
- Chan, T. F., & Vese, L. A. (2001). Active contours without edges. *IEEE Transactions on Image Processing*, 10(2), 266–277. <https://doi.org/http://dx.doi.org/10.1109/83.902291>
- Chan, T. F., Yezriev Sandberg, B., & Vese, L. A. (2000). Active contours without edges for vector-valued images. *Journal of Visual Communication and Image Representation*, 11(2), 130–141. <https://doi.org/http://dx.doi.org/10.1006/jvci.1999.0442>
- Codella, N. C. F., Gutman, D., Celebi, M. E., Helba, B., Marchetti, M. A., Dusza, S. W., Kalloo, A., Liopyris, K., Mishra, N., Kittler, H., & Halpern, A. (2018, April). Skin lesion analysis toward melanoma detection: A challenge at the 2017 International symposium on biomedical imaging (ISBI), hosted by the international skin imaging collaboration (ISIC). In *Proceedings - International Symposium on Biomedical Imaging, 2018-April (ISBI)* (pp. 168–172). <https://doi.org/10.1109/ISBI.2018.8363547>
- Dobrosotskaya, J., & Guo, W. (2017). A PDE-free variational method for multi-phase image segmentation based on multiscale sparse representations. *Journal of Imaging*, 3(3), 1–26. <https://doi.org/10.3390/jimaging3030026>
- Embong, R., Aziz, N. M. N. A., Karim, A. H. A., & Ibrahim, M. R. (2017). Colour application on mammography image segmentation. *Colour Application on Mammography Image Segmentation*, 890(1), 1–8. <https://doi.org/http://dx.doi.org/10.1088/1742-6596/890/1/012066>
- Fang, J., Liu, H., Zhang, L., Liu, J., & Liu, H. (2021). Region-edge-based active contours driven by hybrid and local fuzzy region-based energy for image segmentation. *Information Sciences*, 546, 397–419. <https://doi.org/10.1016/j.ins.2020.08.078>

- Fang, L., Qiu, T., Liu, Y., & Chen, C. (2018). Active contour model driven by global and local intensity information for ultrasound image segmentation. *Computers & Mathematics with Applications*, 75(12), 4286–4299. <https://doi.org/10.1016/j.camwa.2018.03.029>
- Getreuer, P. (2012). Rudin–Osher–Fatemi total variation denoising using split Bregman. *Image Processing on Line*, 2(1), 74–95. <https://doi.org/http://dx.doi.org/10.5201/ipol.2012.g-tvd>
- Hore, S., Chakraborty, S., Chatterjee, S., Dey, N., Ashour, A. S., Van Chung, L., & Le, D. N. (2016). An integrated interactive technique for image segmentation using stack based seeded region growing and thresholding. *International Journal of Electrical and Computer Engineering*, 6(6), 2773–2780. <https://doi.org/http://dx.doi.org/10.11591/ijece.v6i6.pp2773-2780>
- Huang, Y., & Liu, Z. (2015). Segmentation and tracking of lymphocytes based on modified active contour models in phase contrast microscopy images. *Computational and Mathematical Methods in Medicine*, 2015. <https://doi.org/http://dx.doi.org/10.1155/2015/693484>
- Jiang, X., Zhou, Z., Ding, X., Deng, X., Zou, L., & Li, B. (2017). Level set based hippocampus segmentation in MR images with improved initialization using region growing. *Computational and Mathematical Methods in Medicine*, 2017. <https://doi.org/http://dx.doi.org/10.1155/2017/5256346>
- Jumaat, A. K., & Chen, K. (2020). Three-dimensional convex and selective variational image segmentation model. *Malaysian Journal of Mathematical Sciences*, 14(3), 437–450. <https://einspem.upm.edu.my/journal/fullpaper/vol14no3/7.%20Abdul%20Kadir%20Jumaat.pdf>
- Jumaat, A. K., & Chen, K. (2019). A reformulated convex and selective variational image segmentation model and its fast multilevel algorithm. *Numerical Mathematics Theory Methods and Applications*, 12(2), 403–437. <http://dx.doi.org/10.4208/nmtma.OA-2017-0143>
- Jumaat, A. K., & Chen, K. (2017). An optimization-based multilevel algorithm for variational image segmentation models. *Electronic Transactions on Numerical Analysis*, 46, 474–504. <https://etna.ricam.oeaw.ac.at/vol.46.2017/pp474-504.dir/pp474-504.pdf>
- Kass, M., Witkin, A., & Terzopoulos, D. (1988). Snakes: Active contour models. *International Journal of Computer Vision*, 1(4), 321–331. https://www.researchgate.net/publication/284653608_Snakes_Active_Contour_Models

- Li, H., Cai, J., Nguyen, T. N. A., & Zheng, J. (2013, July). A benchmark for semantic image segmentation. In *IEEE International Conference on Multimedia and Expo* (pp. 1–6.) <https://doi.org/10.1109/ICME.2013.6607512>
- Martin, D., Fowlkes, C., Tal, D., & Malik, J. (2001, July). A database of human segmented natural images and its application to evaluating segmentation algorithms and measuring ecological statistics. In *Proceedings Eighth IEEE International Conference on Computer Vision. ICCV 2001*, (Vol. 2, pp. 416–423). <https://doi.org/http://dx.doi.org/10.1109/ICCV.2001.937655>
- Mazouzi, S., & Guessoum, Z. (2021). A fast and fully distributed method for region-based image segmentation: Fast distributed region-based image segmentation. *Journal of Real-Time Image Processing*, 18(3), 793–806. <https://doi.org/10.1007/s11554-020-01021-7>
- Moreira, I. C., Amaral, I., Domingues, I., Cardoso, A., Cardoso, M. J., & Cardoso, J. S. (2012). INbreast: Toward a full-field digital mammographic database. *Academic Radiology*, 19(2), 236–248. <https://doi.org/10.1016/j.acra.2011.09.01414>
- Mumford, D., & Shah, J. (1989). Optimal approximations by piecewise smooth functions and associated variational problems. *Communications on Pure and Applied Mathematics*, 42(5), 577–685. <https://doi.org/http://dx.doi.org/10.1002/cpa.3160420503>
- Nguyen, T., Cai, J., Member, S., IEEE, Zhang, J., & Zheng, J. (2012). Robust interactive image segmentation using convex active contours. *IEEE Transactions on Image Processing*, 21(8), 3734–3743. <https://doi.org/http://dx.doi.org/10.1109/TIP.2012.2191566>
- Osher, Stanley, J., & Sethian, J. (1988). Fronts propagating with curvature-dependent speed: Algorithms based on Hamilton-Jacobi formulations. *Computational Physics*, 79(1), 1–5. <https://doi.org/http://dx.doi.org/10.1016/0021-9991%2888%2990002-2>
- Othman, M., Abdullah, S. L. S., Ahmad, K. A., Bakar, M. N. A., & Mansor, A. R. (2016). The fusion of edge detection and mathematical morphology algorithm for shape boundary recognition. *Journal of Information and Communication Technology (JICT)*, 15(1), 133–144. <http://e-journal.uum.edu.my/index.php/jict/article/view/8175>

- Rada, L., & Chen, K. (2011). A new variational model with dual level set functions for selective segmentation. *Communications in Computational Physics*, 12(1), 261–283. <https://doi.org/https://doi.org/10.4208/CICP.190111.210611A>
- Rada, L., & Chen, K. (2013). Improved selective segmentation model using one level-set. *Journal of Algorithms & Computational Technology*, 7(4), 509–540. <https://doi.org/http://dx.doi.org/10.1260/1748-3018.7.4.509>
- Shaker, F., Monadjemi, S. A., Alirezaie, J., & Naghsh-Nilchi, A. R. (2017). A dictionary learning approach for human sperm heads classification. *Computers in Biology and Medicine*, 91, 181–190. <https://doi.org/http://dx.doi.org/10.1016/j.combiomed.2017.10.009>
- Shi, Y., Li, M., & Zeng, W. (2021). MARGM: A multi-subjects adaptive region growing method for group fMRI data analysis. *Biomedical Signal Processing and Control*, 69 (November 2020), 102882. <https://doi.org/10.1016/j.bspc.2021.102882>
- Spencer, J., & Chen, K. E. (2015). A convex and selective variational model for image segmentation. *Communications on Mathematics and Sciences*, 13(6), 1453–1472. <https://doi.org/http://dx.doi.org/10.4310/CMS.2015.v13.n6.a5>
- Vese, L. A., & Chan, T. F. (2002). A multiphase level set framework for image segmentation using the Mumford and Shah Model. *International Journal of Computer Vision*, 50(3), 271–293. <https://doi.org/http://dx.doi.org/10.1023/A:1020874308076>
- Wei, W. B., Tan, L., Jia, M. Q., & Pan, Z. K. (2017). Normal vector projection method used for convex optimization of Chan-Vese model for image segmentation. *Journal of Physics: Conference Series*, 787, Article 012016. <https://iopscience.iop.org/article/10.1088/1742-6596/787/1/012016>
- Xu, C., & Prince, J. L. (1998). Snakes, shapes, and gradient vector flow. *IEEE Transactions on Image Processing*, 7(3), 359–369. <https://doi.org/http://dx.doi.org/10.1109/83.661186>
- Xue, Y., Zhao, J., & Zhang, M. (2021). A watershed-segmentation-based improved algorithm for extracting cultivated land boundaries. *Remote Sensing*, 13(5), 1–19. <https://doi.org/10.3390/rs13050939>
- Yearwood, A. B. (2018). *A brief survey on variational methods for image segmentation* (Research Assignment: Chicago Referencing). ResearchGate. https://www.researchgate.net/publication/323971382_A_Brief_Survey_on_Variational_Methods_for_Image_Segmentation

- Yue, W. (2009). *A simple introduction of active contour without edges*. <https://sites.google.com/s24ite/rexstribeofimageprocessing/chan-vese-active-contours/wubiaotitiezi>
- Zhang, Y., Guo, H., Chen, F., & Yang, H. (2017). Weighted kernel mapping model with spring simulation based watershed transformation for level set image segmentation. *Neurocomputing*, 249, 1–18. <https://doi.org/http://dx.doi.org/10.1016/j.neucom.2017.01.044>
- Zhao, W., Xu, X., Zhu, Y., & Xu, F. (2018). Active contour model based on local and global Gaussian fitting energy for medical image segmentation. *Optik*, 158, 1160–1169. <https://doi.org/10.1016/j.ijleo.2018.01.004>